Thermalization of an intense, space-charge-dominated electron beam in a long focusing channel

Bruce E. Carlsten
Los Alamos National Laboratory, Los Alamos, New Mexico 87545
(Received 29 January 1999)

A continuous electron beam with a correlated emittance will eventually thermalize. Initially, the beam emittance for an intense, high-brightness, space-charge-dominated beam will oscillate, but after a sufficiently long time, it will reach an equilibrium value. The emittance oscillations are due to coherent transverse plasma oscillations in the beam and are a manifestation of periodic energy exchange between potential and kinetic energies. The beam eventually attains an equilibrium emittance, as the beam equipartitions the kinetic and potential energies. This equipartioning is reached as the beam thermalizes due to a form of Landau damping of the radial oscillations at different radial positions within the beam. Slight differences in the transverse plasma oscillation frequency for different radial positions lead to incoherence in the oscillations. In this paper, we calculate the equilibrium time scales required for equipartioning. We show that the equilibrium emittance scalings and magnitude can be predicted by conservation of energy considerations. In addition, we show that, in the space-charge dominated regime, there is a correspondence between the energy-conservation approach and the kinematic approach. [S1063-651X(99)10608-1]

PACS number(s): 03.50.De, 29.27.Bd, 41.75.Ht

I. INTRODUCTION

High-current, low-emittance, high-brightness, space-charge-dominated electron beams in long focusing channels often demonstrate emittance oscillations, where the rms, normalized radial beam emittance is defined by

$$\varepsilon = 2\beta\gamma\sqrt{\langle r^2\rangle\langle r'^2\rangle - \langle rr'\rangle^2}, \tag{1}$$

where the brackets refer to ensemble averages over the particle distribution at a single axial location, β is the beam's axial velocity normalized to the speed of light, γ is the relativistic mass factor, r is the radial coordinate of the particles, and the prime refers to an axial derivative. Although this is not a strictly conserved quantity (it does not grow in an axial magnetic field), this is an appropriate emittance definition here because we will assume that the beam has no initial thermal emittance and that the beam has zero canonical angular momentum. The emittance is a direct measure of the beam's quality [1], and the definition here keeps it unambiguous while the beam is in an external axial magnetic field [2].

Emittance oscillations are common in rf photoinjectors [3–6] and other high-brightness electron beams. The emittance growth is due to mismatches between particles' injection conditions and their equilibrium orbits. These mismatches can be caused by a nonequilibrium beam density, nonlinear transverse forces in a gun or focusing section, or other nonlinearities. The emittance growth results from radial nonlinearities in the particles' oscillations about their equilibrium radii. To first order, these orbit oscillations are in phase, and the emittance growth vanishes at intervals of half plasma periods, and is thereby periodic. These emittance oscillations have been analyzed in detail for rf photoinjectors [5,6]. For rf photoinjectors, the beam is rapidly accelerated, and only goes through a few emittance oscillations by the time it reaches its final application, due to the time dilation of a relativistic beam and the high accelerating gradient. However, a large number of these oscillations could occur for an emerging class of high-brightness, low-gradient, high-current induction linacs with long-pulse electron beams [7,8].

It is important to point out that these emittance oscillations do not occur for several classes of charged particle beams, including most ion beams and low-brightness electron beams. For these types of beams, the initial mismatch leads to an emittance growth that asymptotes to a final value and does not oscillate. This occurs when there is overtaking, or wave breaking, in radial phase space. This overtaking takes place within a quarter transverse plasma period, and transforms an initially simply correlated emittance to one that is not simply correlated and effectively unrecoverable, and thus its magnitude will not oscillate. The split between these regimes will be more clearly defined in the Appendix. For the purposes of this paper, we will call the regime where no wave breaking occurs to be space-charge dominated and the regime where wave breaking occurs to be emittance dominated. Note that these are not the usual definitions, but these definitions are more relevant to this study. The emittance evolution in the emittance-dominated regime can be described well by thermodynamic considerations and is formally well understood [1]. It is the purpose of this paper to present an equivalent understanding of the emittance evolution in the space-charge dominated regime where these emittance oscillations occur.

Over a sufficiently long distance, these emittance oscillations will damp out, leading to an effective thermalized emittance, at an intermediate value. A typical simulation is shown in Fig. 1, of a 4-kA, 4-MeV, long-pulse electron beam with a 3-cm radius, using the particle-pushing code SLICE [9]. We see several (on the order of 30) oscillations, gradually decaying in amplitude to an intermediate value, followed by some minor emittance oscillations due to beating.

In this simulation, an initially zero-emittance beam, with nonuniform charge density, was injected into a transport channel with a constant external magnetic field. The external

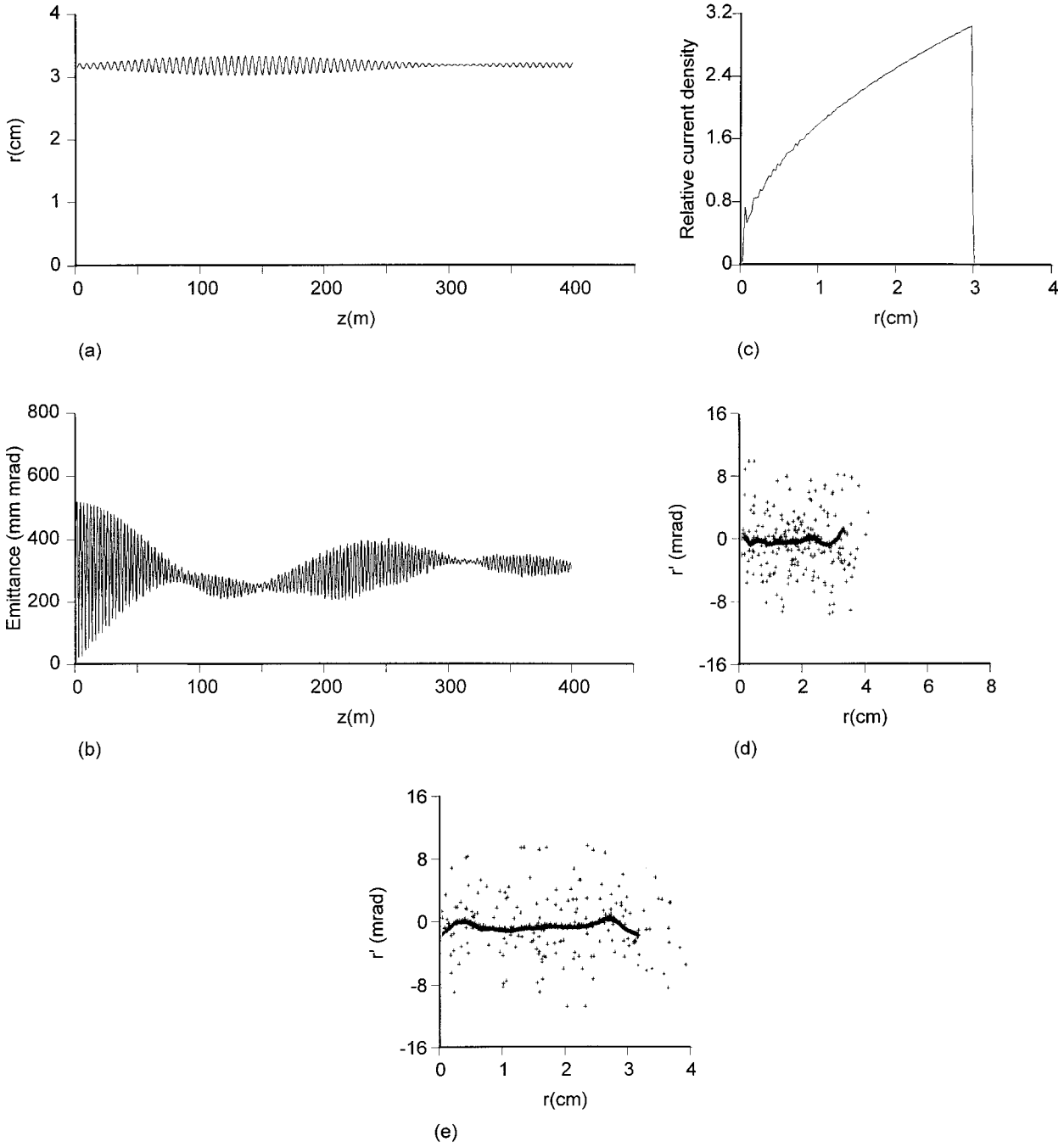

FIG. 1. (a) Beam rms radius versus axial distance, nominal case (4 MeV, 4 kA); (b) emittance versus axial distance, nominal case; (c) initial beam density; (d) final beam radial phase space; and (e) beam radial phase space at 375 m.

field was adjusted so that the beam rms radius was nearly matched. The beam was assumed to have zero canonical angular momentum. The beam energy was 4 MeV and beam current was 4 kA. This problem geometry was chosen to unambiguously demonstrate the important physics of the emittance oscillations and equipartioning. The SLICE code self-consistently pushes particles using the Lorentz force equation, including the beam's self radial electric and axial magnetic field (the beam's diamagnetic field). Busch's theorem [10] is used to calculate the azimuthal motion of the particles. The code uses the long-beam approximation, in which Gauss's law is used for the radial electric field and Ampere's law is used for the axial magnetic field. A collection of particles at the same axial location is used to describe the beam. As a group, the particles are stepped axially from the origin to the end of the problem. For these simulations, a 0.2-mm axial step size and 16 000 particles per axial slice were used to ensure sufficient numerical stability.

In this simulation and the following analysis we have initiated the beam mismatch with a nonuniform beam density. In more realistic cases, the mismatch occurs from a combination of nonuniform beam density and nonlinear external focusing forces. However, the phenomena described in this paper are mostly independent of the exact cause of the mismatch and also occur for mismatches due to nonlinear focusing.

For the nominal case, we have chosen a density nonuniform of about 100% (as defined in the following analysis), in

order to generate emittances of several hundred mm mrad which is typical for new and proposed high-brightness induction accelerators. The following analysis assumes relatively small density nonuniformities; however, the analysis gives proper scaling laws and even relatively good quantitative estimates when compared to the simulations (within a factor of two). Also, we have assumed that the density profile is linear with radius. This was done because a more general density function would lead to essentially the same results as found here, with some slightly different numerical factors. This approximation allows us to simply characterize the beam density nonuniformity with a single parameter in order to make an approximate estimate of the emittance evolution.

We have plotted in Fig. 1 the simulation results for the nominal case, described above, for an overall transport distance of 400 m. In Fig. 1(a), we see the beam rms radius versus axial distance. In Fig. 1(b), we see the beam rms emittance versus axial distance. In Fig. 1(c), we see the beam's initial current density as a function of radial position, and in Fig. 1(d) we see the final beam phase space $r-r'$. In Fig. 1(e), we see the beam phase space at a second, slightly different axial location (375 m).

We see four key features in this simulation. First, we see very pronounced large emittance oscillations at short axial distances. Second, these oscillations damp out to an equilibrium emittance somewhat larger than the mean of the oscillations. Third, the equilibrium emittance is stable over very long axial distances. Fourth, although the equilibrium emittance is approximately constant, the beam phase space is changing, with kinks moving up and down the particle phase-space distribution.

We will explain these features in this paper, for beams in the space-charge-dominated regime. As described above, the emittance oscillations arise from coherent transverse plasma oscillations within the beam. However, the phase of the oscillations vary slightly at different radial positions, and the oscillations are thus Landau damped to a stable equilibrium value. This equilibrium emittance is a thermalized, but correlated emittance, as seen in Figs. 1(d) and 1(e). Long-term beating of the collection of slightly different frequencies account for the slight re-emergence of the emittance oscillations.

Both the peak of the emittance oscillations and the equilibrium emittance scale linearly with beam radius, linearly with the square root of the current, and inversely with the square root of the relativistic mass factor.

In addition to wave breaking in phase space for emittance-dominated beams, this emittance-oscillation mechanism is not relevant if collisions between particles thermalize the beam in a short distance. However, for these types of beams, the collisional mechanism requires thousands of meters for thermalization, and is not significant.

Another important conclusion in this paper is that, in the space-charge-dominated regime, a kinematic analysis of the beam emittance evolution is equivalent to an analysis based on energy conservation. This correspondence is not true in general for emittance-dominated electron beams.

In the next section, we verify that the thermalization distance due to collisions between particles is extremely long. In the following section, we estimate the axial distance required for Landau damping by considering the range of transverse plasma oscillation frequencies at different radial locations within the beam.

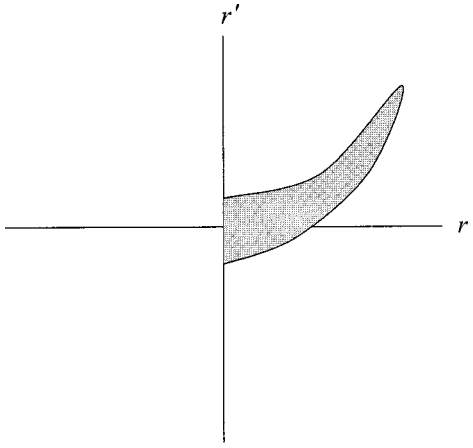

FIG. 2. Hypothetical beam radial phase space, showing both correlated and uncorrelated parts to the emittance.

Then we describe the emittance growth from the point of view of the excess potential energy of the system, and predict both the maximum of the emittance oscillations and the thermalized emittance. These predictions are in good agreement with the simulations in terms of both absolute magnitudes and scalings with beam parameters. We consider the effect of radial correlations in the emittance growth, and show that both the energy-conservation and kinematic approaches yield equivalent results.

In the final section, we show that any long-term emittance decay or growth must be on extremely long axial scales.

II. THERMALIZATION DUE TO COLLISIONS BETWEEN PARTICLES

In this section we estimate the scale lengths required for the beam's phase space to reach thermal equilibrium resulting from Coulomb collisions between particles, and show that this mechanism is insignificant over the axial distances we are considering. We consider the phase space shown in Fig. 2. There is a correlated beam emittance with some small uncorrelated component. We consider purely transverse Coulomb collisions between particles that are slightly radially offset, as shown in Fig. 3. This type of collision transfers transverse energy to transverse energy. This class of collisions is the dominant one leading to transverse thermalization, and will lead to an increase of the uncorrelated emittance, until an equilibrium level is reached. The mechanism can be understood by considering Figs. 2 and 3. Particles at slightly different radial positions, but with some uncorrelated emittance, will undergo radial Coulomb scatterings, which will tend to give particles at nearby radial positions the same rms radial divergence. Slowly, the beam's phase space will evolve so that the radial rms divergence is the same at all radial positions within the beam. The interacting particles, shown in Fig. 3, initially have identical angular momentum, but a relative radial velocity due to the uncorrelated emittance. There are no scatterings without the uncorrelated emittance; the rate of thermalization depends on the magnitude of the uncorrelated emittance. Note that this mechanism will

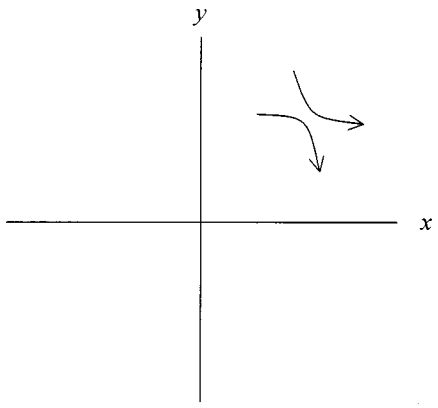

FIG. 3. Radial Coulomb collision between two particles due to uncorrelated emittance.

also lead to an uncorrelated spread in azimuthal velocities, which will slightly modify the transfer rate of radial divergence between radial positions, as we will see below.

Alternative scattering mechanisms are not important. Relativistic beams have very little axial velocity spread, and the transfer from axial energy to transverse energy is insignificant. Also, transverse collisions that transfer transverse energy to axial energy (the Boersch effect [11–13]) provide some damping of the transverse energy, but do not change the thermalization scale length at the level we are calculating.

The thermalization rate from transverse collisions will slow down, as the transverse energy at a given radial position grows to the equilibrium value, due to equilibrium forces. We will not consider these equilibrium forces, and just estimate the equilibrium time by dividing the equilibrium transverse energy by the initial transverse energy growth rate. This will underestimate the equilibrium distance, but can be used to show that this mechanism is unimportant for typical high-brightness, relativistic beams. We will assume that the beam is mostly uniform in density.

The transverse momentum transfer for the two particles in Fig. 3 in their center-of-mass frame is given by

$$\Delta p_{\mathrm{c.m.}}=\frac{2e^2}{\nu_{\mathrm{rel}} b 4\pi\varepsilon_0}, \tag{2}$$

where b is their impact parameter, e is the electronic charge, ε_0 is the permitivity of free space, and ν_{rel} is the particles' relative velocity in their frame of reference. The average energy transfer is very small for any particle, but the average energy transfer rate does not have to be. The transverse velocity transfer is given by

$$(\Delta\nu)^2_{\mathrm{c.m.}}=\frac{4e^4}{m^2\nu_{\mathrm{rel}}^2 b^2(4\pi\varepsilon_0)^2}, \tag{3}$$

where now m is the electronic mass. Now the number of collisions per second that a single electron sees in its center-of-mass frame is given by

$$d\left(\frac{\mathcal{N}_{\mathrm{c.m.}}}{\mathrm{sec}}\right)=\frac{I}{\pi r_e^2\beta\gamma ce}\,\nu_{\mathrm{rel}}(2\pi b)db, \tag{4}$$

where $\mathcal{N}$ is the number of collisions, I is the beam current, and r_e is the beam edge radius.

The rate of increase in the transverse rms velocity transfer is thus given by

$$\frac{d(\Delta\nu)^2_{\mathrm{c.m.}}}{dt_{\mathrm{c.m.}}}=\int\frac{8Ie^3}{r_e^2\beta\gamma cm^2\nu_{\mathrm{rel}} b(4\pi\varepsilon_0)^2}db. \tag{5}$$

After integration over all impact parameters and transferring variables to the beam frame ($\Delta\nu_{\mathrm{lab}}=\Delta\nu_{\mathrm{cm}}/\gamma$, $\nu_{\mathrm{lab}}=\nu_{\mathrm{rel}}/\gamma$, and $t_{\mathrm{lab}}=t_{\mathrm{cm}}\gamma$), we have

$$\frac{d(\Delta\nu)^2_{\mathrm{lab}}}{dt}=\frac{8Ie^3c^5}{r_e^2\beta\gamma^5c^6m^2\nu_{\mathrm{lab}}(4\pi\varepsilon_0)^2}\ln\Lambda$$
$$=\frac{8Iec^5}{I_A^2r_e^2\beta\gamma^5\gamma_{\mathrm{lab}}}\ln\Lambda, \tag{6}$$

where we have used $I_A=mc^3 4\pi\varepsilon_0/e$, which is about 17 kA, and the logarithm of the ratio of allowable impact parameters is always close to 10 [1].

The beam's unnormalized emittance is $\varepsilon^2_{\mathrm{un}}=[\Delta\nu^2_{\mathrm{lab}}/\beta^2c^2]r_e^2$ (the missing factor of 2 results from equipartitioning between the radial and azimuthal directions), and the normalized emittance is related to the unnormalized emittance by $\varepsilon_n^2=\varepsilon^2_{\mathrm{un}}/\beta^3\gamma^3$. Note that the rms relative velocity is given by $\varepsilon_{\mathrm{un}}=r_e\nu_{\mathrm{lab}}/\beta c$. The unnormalized emittance growth is given by

$$\frac{d\varepsilon^2_{\mathrm{un}}}{dt}=\frac{8Iec^2r_e}{I_A^2\gamma^5\beta^3\varepsilon_{\mathrm{un}}}\ln\Lambda \tag{7}$$

and the normalized emittance growth is given by

$$\varepsilon_n^3=z\frac{24Iecr_e}{I_A^2\gamma^2\beta^2}\ln\Lambda. \tag{8}$$

For a beam of about 4 kA and a relativistic mass factor of about 10, over a kilometer is required for an emittance growth of 100 mm mrad.

III. ESTIMATING TIME REQUIRED FOR THERMALIZATION DUE TO LANDAU DAMPING

We can estimate the time required for the Landau damping to occur, by considering the spread of the periods of the transverse plasma oscillations.

The beam is space-charge-dominated, and we will assume that the particle motion is laminar with no particle orbits crossing. The transverse motion of a particle in a slice of the beam in a uniform focusing channel of normalized strength K is given by

$$\sigma''+K\sigma-\frac{\hat{K}_s}{\sigma}=0, \tag{9}$$

where σ is the transverse coordinate of the particle and $\hat{K}_s$ is the normalized space-charge force, $\hat{K}_s=2I(r)/I_A\gamma^3\beta^3$, where $I(r)$ is the current enclosed by the particle's orbit. The equilibrium particle radius is given by

$$\sigma_{\rm eq}=\sqrt{\hat{K}_s/K}. \tag{10}$$

We write the particle radius as

$$\sigma=\delta+\sigma_{\rm eq}, \tag{11}$$

and we assume that all particles in the beam are very nearly matched to their equilibrium orbits (the beam is rms matched and the density nonuniformity is small). We then come up with this differential equation for the displacement:

$$\delta''+\left[2K+K\left(\frac{\delta}{\sigma_{\rm eq}}\right)^2\right]\delta-K\left(\frac{\delta}{\sigma_{\rm eq}}\right)^2\sigma_{\rm eq}=0. \tag{12}$$

For small displacements, we can substitute $(\delta_{\rm rms}/\sigma_{\rm eq})^2$ for $(\delta/\sigma_{\rm eq})^2$, and this equation has the solution

$$\delta=\delta_0+\delta_1\cos\Omega z, \tag{13}$$

where

$$\Omega=K^{1/2}\left[2+\left(\frac{\delta_{\rm rms}}{\sigma_{\rm eq}}\right)^2\right], \tag{14}$$

$$\delta_0=\frac{K\left(\frac{\delta_{\rm rms}}{\sigma_{\rm eq}}\right)^2}{2K+K\left(\frac{\delta_{\rm rms}}{\sigma_{\rm eq}}\right)^2}\sigma_{\rm eq}, \tag{15}$$

and δ_1 is given by the initial offset from the particle's equilibrium position. Equations (13) and (15) can be solved to find the particle's orbit exactly to this order; however, for estimating the time required for Landau damping, this is not necessary.

Note that the equilibrium orbit radius is given by $\sigma_{\rm eq}=r\sqrt{J/J_{\rm rms}}$, where r is the particle injection radius, J is the average current density up the particle's orbit, and $J_{\rm rms}$ is the rms current density. The initial orbit offset is given by $\delta_0=\sigma_{\rm eq}(1-\sqrt{J_{\rm rms}/J})$, and the rms offset is close to $\delta_{\rm rms}^2=\delta_0^2/2$. The particle's oscillation frequency is given by

$$\Omega(r)=K^{1/2}[2+\tfrac{1}{2}(\sqrt{J_{\rm rms}/J}-1)^2]. \tag{16}$$

At small axial locations, the particles' oscillations stay in phase, resulting in the coherent transverse oscillations leading to the emittance oscillations shown in Fig. 1(b).

The transverse oscillations are out of phase at an axial location $z_{\rm Landau}$ when the oscillations of the rms trajectory and the edge trajectory are 90 degrees out of phase:

$$\{(2K)^{1/2}[1+\tfrac{1}{4}(\sqrt{J_{\rm rms}/J}-1)^2]-(2K)^{1/2}\}z_{\rm Landau}=\frac{\pi}{2} \tag{17}$$

or

$$\frac{z_{\rm Landau}}{z_{\rm plasma}}=\frac{1}{(\sqrt{J_{\rm rms}/J}-1)^2}, \tag{18}$$

where $z_{\rm plasma}$ is the distance required for a plasma oscillation,

$$z_{\rm plasma}=2\pi/(2K)^{1/2}=\pi r_e\sqrt{(I/I_A)\gamma^3\beta^3}. \tag{19}$$

For the density variation in Fig. 1 ($J_{\rm rms}/J$ about 0.7), this formula predicts that the equilibrium is reached in about 30 plasma oscillation periods; from Fig. 1(b), we see that equilibrium is reached in about 35 periods. This agreement shows that the Landau damping model is consistent with the simulation. Examination of the final phase-space plot [Fig. 1(c)] shows that different parts of the slice are at different phases of the oscillations. A second phase-space plot, a little bit upstream [Fig. 1(e)], shows that the oscillation phases of different slice locations have changed, but the rms emittance is basically unchanged.

Note that the plasma wavelength for the nominal case is 5.1 m, or the emittance oscillation period is about 2.55 m, in excellent agreement with that shown in Fig. 1(b)

IV. ESTIMATING THE MAXIMUM EMITTANCE AND THE EQUILIBRIUM EMITTANCE FROM ENERGY CONSERVATION ARGUMENTS

In the space-charge-dominated regime, the emittance growth is mostly due to the radial velocity of the particles, and the effect of the radial positions can be neglected. The short-range emittance oscillations have the following features. Initially, there is no emittance, as the radial velocity is zero, but there are nonlinear forces on the particles. These nonlinear forces (which vanish in an rms sense) lead to nonlinear radial particle velocities, and an emittance growth. The emittance increases as long as the nonlinear force is in the same direction. However, the nonlinear forces decrease as the particle motion tends to lead the beam to a uniform density distribution. When the distribution reaches the equilibrium, uniform density, the nonlinear forces vanish, but the nonlinear radial velocities are at a maximum. At this point, the emittance has grown to its maximum value. As the particle distribution becomes nonuniform in the opposite sense that it was initially, the reversed nonlinear forces lead to a lessening of the nonlinear radial velocities, and an emittance decrease. Within this model, the beam density distribution will oscillate about the equilibrium distribution, with concurrent emittance oscillations.

From this model, it is easy to estimate both the maximum of the emittance oscillations and the equilibrium emittance after Landau damping, from conservation of energy arguments. This approach is closely related to the nonlinear free-energy approach [1,14,15] to estimate the emittance growth in emittance-dominated beams, but with some differences, which we will outline below. As pointed out in the nonlinear free-energy analysis, the nonuniform beam has a greater average energy per particle than a uniform distribution with equal rms size. As the beam density becomes uniform due to the nonlinear space-charge forces, the emittance can be found by equating the rms radial energy to the initial excess space-charge potential of the beam, resulting from the conservation of total beam energy.

Another approach is to calculate the initial emittance growth rate using kinematic equations, and to calculate the magnitude of the emittance oscillation assuming that the emittance oscillation period is given by one-half a plasma period. Both approaches result in an equivalent value for the maximum emittance.

The equilibrium emittance can be found by assuming that

at equilibrium, half the initial excess energy is in radial motion and half in stored potential energy. Thus, the equilibrium emittance is $1/\sqrt{2}$ times the maximum emittance in the early emittance oscillations (ignoring radial correlations). This relationship is confirmed in Fig. 1(b).

The physics associated with this effect is related to, but somewhat different than that if the beam is in the emittance-dominated regime. In that case, as the beam relaxes to a uniform distribution, the emittance causes a reordering of particles via wave breaking in phase space, and the coherence is lost. As a result, all the emittance growth over a quarter plasma period remains. Another way to think about this is that all the excess energy ends up in radial motion because the decoherence of the beam due to the emittance prevents any long-term stored potential energy.

A. Initial excess potential energy

We will simplify the calculation of the excess potential energy of the initial, nonuniform beam if we assume that the charge density profile can be expressed by

$$\rho(r)=\rho_0+\rho_1 r, \tag{20}$$

up to a beam edge radius of r_e, and zero beyond. A uniform beam with the same current and beam edge radius has density $\rho_c=\rho_0[1+2/3(\rho_1 r_e/\rho_0)]$. The radial electric field from the space charge is given by

$$E_r=\frac{\rho_0}{2\varepsilon_0}r\left(1+\frac{2}{3}\frac{\rho_1 r}{\rho_0}\right). \tag{21}$$

The radial space-charge force is given by

$$F_r=\frac{\rho_0}{2\gamma^2\varepsilon_0}r\left(1+\frac{2}{3}\frac{\rho_1 r}{\rho_0}\right) \tag{22}$$

and the radial focusing force from the external solenoid that would keep the uniform density beam in equilibrium is given by

$$F_{\text{ext}}=-\frac{\rho_0}{2\gamma^2\varepsilon_0}r\left(1+\frac{2}{3}\frac{\rho_1 r_e}{\rho_0}\right). \tag{23}$$

The net force is given by

$$F_{\text{total}}=\frac{\rho_1}{3\gamma^2\varepsilon_0}r(r-r_e). \tag{24}$$

In Eqs. (21)–(24), we have neglected the small nonlinear component resulting from the nonlinear part of the axial diamagnetic field [9]. This term has an additional factor I/I_A, and, for the nominal case, causes only about a 10% effect, and is considered insignificant.

Note that we have set up this problem so that the beam edge radius will not change, but the density will vary within it, to simplify the stored energy arguments.

In order to calculate the average excess potential energy, we need to calculate the average potential energy for both the nonuniform density case and the corresponding uniform density case. We will do this using the prescription in [1], where the total potential energy of the beam is given by

$$W_{\text{total}}=W_{\text{ext}}+W_{\text{sc},E}-W_{\text{sc},B}=W_{\text{ext}}+\frac{W_{\text{sc},E}}{\gamma^2}, \tag{25}$$

where W_{ext} is the potential energy due to the external focusing, $W_{\text{sc},E}$ is the potential energy due to the space-charge electric field, and $W_{\text{sc},B}$ is the potential energy due to the space-charge magnetic field. We will use W to refer to the total energy of the beam per unit length and per unit radian (so we only have to perform the radial integration) and U to refer to the average energy per particle. Note that the number of particles per unit length and per radian is

$$N=\frac{\int_0^{r_e}(\rho_0+\rho_1 r)r\,dr}{e}=\frac{\rho_0\left(1+\frac{\rho_1 r_e}{\rho_0}\right)r_e^2}{2e}. \tag{26}$$

The external potential is given by

$$V_{\text{ext}}=\frac{\rho_0}{4\gamma^2\varepsilon_0}r^2\left(1+\frac{2}{3}\frac{\rho_1 r_e}{\rho_0}\right), \tag{27}$$

and the potential energy from the external focusing is given by

$$W=\int_0^{r_e}\rho(r)V_{\text{ext}}r\,dr. \tag{28}$$

For the nonuniform case, this leads to

$$W_{\text{ext,non}}=\frac{\rho_0^2}{16\gamma^2\varepsilon_0}\left[1+\left(\frac{2}{3}+\frac{4}{5}\right)\left(\frac{\rho_1 r_e}{\rho_0}\right)+\frac{8}{15}\left(\frac{\rho_1 r_e}{\rho_0}\right)^2\right], \tag{29}$$

and

$$W_{\text{ext,un}}=\frac{\rho_0^2}{16\gamma^2\varepsilon_0}\left[1+\frac{4}{3}\left(\frac{\rho_1 r_e}{\rho_0}\right)+\frac{4}{9}\left(\frac{\rho_1 r_e}{\rho_0}\right)^2\right] \tag{30}$$

for the uniform case.

The stored energy from the space-charge electric field is given by

$$W_{\text{sc}}=\frac{\varepsilon_0}{2}\int_0^{r_e}E_r^2 r\,dr, \tag{31}$$

where E_r is from Eq. (21). The net space-charge potential energy for the nonuniform case is then given by

$$W_{\text{sc},E,\text{non}}-W_{\text{sc},B,\text{non}}=\frac{\rho_0^2}{32\gamma^2\varepsilon_0}\left[1+\frac{16}{15}\left(\frac{\rho_1 r_e}{\rho_0}\right)+\frac{16}{54}\left(\frac{\rho_1 r_e}{\rho_0}\right)^2\right]. \tag{32}$$

The potential energy for the equilibrium case (letting ρ_1 go to zero and ρ_0 go to ρ_c) is given by

$$W_{\text{sc},E,\text{un}}-W_{\text{sc},B,\text{un}}=\frac{\rho_0^2}{32\gamma^2\varepsilon_0}\left[1+\frac{4}{3}\left(\frac{\rho_1 r_e}{\rho_0}\right)+\frac{4}{9}\left(\frac{\rho_1 r_e}{\rho_0}\right)^2\right]. \tag{33}$$

The excess energy per unit length and unit radian is thus given by

$$W_{\text{total,non}} - W_{\text{total,un}} = \frac{\rho_0^2}{16\gamma^2\varepsilon_0}\left(\frac{4}{45} - \frac{2}{27}\right)\left(\frac{\rho_1 r_e}{\rho_0}\right)^2. \quad (34)$$

The term linear in the differential density ρ_1 vanishes, as it must, since the uniform-density case has the minimum potential energy.

Using Eq. (26), the average excess energy per particle is now

$$U_{\text{excess}} = \frac{e\rho_0 r_e^2}{\gamma^2\varepsilon_0\left(1 + \frac{2\rho_1 r_e}{3\rho_0}\right)} \frac{1}{540}\left(\frac{\rho_1 r_e}{\rho_0}\right)^2. \quad (35)$$

Note that since $\rho_0 r_e^2$ is proportional to the beam current, the excess energy per particle is independent of the beam radius, and only depends on the beam current and the density nonuniformity. This is not unexpected, since it is the same scaling as the beam's potential depression.

When the distribution is uniform and the emittance is a maximum, all this energy per particle is kinetic, so

$$\left\langle \frac{1}{2}\gamma m \dot{r}^2 \right\rangle = \frac{e\rho_0 r_e^2}{\gamma^2\varepsilon_0\left(1 + \frac{2\rho_1 r_e}{3\rho_0}\right)} \frac{1}{540}\left(\frac{\rho_1 r_e}{\rho_0}\right)^2, \quad (36)$$

or

$$\langle r'^2 \rangle = \frac{e\rho_0 r_e^2}{\gamma^3 m\beta^2 c^2\varepsilon_0\left(1 + \frac{2\rho_1 r_e}{3\rho_0}\right)} \frac{1}{270}\left(\frac{\rho_1 r_e}{\rho_0}\right)^2. \quad (37)$$

The current is given by

$$I = \nu_0\rho_0\pi r_e^2\left(1 + \frac{2\rho_1 r_e}{3\rho_0}\right), \quad (38)$$

which we use to eliminate the constant density term. Assuming that the divergence is uncorrelated with radius (we will quantify this error in the next section), the maximum radial, rms emittance is

$$\varepsilon_{\text{uncorrelated}} = 2\gamma\beta\sqrt{\langle r^2\rangle\langle r'^2\rangle} = \frac{2}{\sqrt{135}\left(1 + \frac{2\rho_1 r_e}{3\rho_0}\right)} \sqrt{(I/I_A\gamma\beta)}\frac{\rho_1 r_e^2}{\rho_0}. \quad (39)$$

The emittance at equilibrium is $1/\sqrt{2}$ times this maximum emittance, as discussed earlier.

Equation (39) predicts a normalized, rms emittance for the nominal case shown in Fig. 1 of 581 mm mrad, with an effective beam nonuniformity of 130% [Fig. 1(c)]. This is a very reasonable estimate [comparing to Fig. 1(c)], but the approximation that the charge density nonuniformity is linear probably limits its quantitative accuracy to 50% or so.

A key point is that radial correlations survive in the space-charge dominated regime—in the emittance dominated regime, correlations between r and r' average to zero.

B. Estimate from initial emittance growth rate

We can also estimate the maximum emittance kinematically from the initial growth rate and knowing that the emittance oscillates at twice the plasma frequency. The initial increase in the emittance is from the nonlinear force, Eq. (24),

$$m\gamma\frac{\Delta\dot{r}}{\Delta t} = \frac{e\rho_1}{3\gamma^2\varepsilon_0} r(r - r_e), \quad (40)$$

or

$$\Delta r' = \Delta z \frac{e\rho_1}{\gamma^3 m\nu_0^2 3\varepsilon_0} r(r - r_e). \quad (41)$$

The ensemble averages for the radial emittance [defined in Eq. (1)] can be easily done, and we find

$$\frac{d\varepsilon_{\text{rms}}}{dz} = \frac{4e\rho_1 r_e^3}{3\sqrt{240}\gamma^2 m\beta c^2\varepsilon_0}\sqrt{2/5}. \quad (42)$$

We have written the correlation term (the $\sqrt{\frac{2}{5}}$) separately to see the effect of the radial correlations for this model. The error in ignoring the correlations is to overestimate the maximum emittance by about 58%.

Note that the magnitude of the emittance oscillates with half a plasma wavelength, but that the emittance grows from zero to maximum in a quarter plasma period. Thus we assume that over a half plasma wavelength the emittance obeys

$$\varepsilon_{\text{rms}} = \varepsilon_{\max}\sin\left(\frac{2\pi z}{\lambda_p}\right), \quad (43)$$

or

$$\frac{d\varepsilon_{\text{rms}}}{dz} = \frac{2\pi}{\lambda_p}\varepsilon_{\max}\cos\left(\frac{2\pi z}{\lambda_\varepsilon}\right). \quad (44)$$

Setting $z = 0$ and equating this to Eq. (42), we immediately find

$$\varepsilon_{\max} = \frac{2r_e}{\sqrt{135}\gamma^{1/2}\beta^{1/2}}\left(\frac{\rho_1 r_e}{\rho_0}\right)\left(\frac{I}{I_A}\right)^{1/2}\sqrt{\frac{2}{5}}. \quad (45)$$

This is the same result as we found previously, but with the additional correction factor due to the radial correlations that exist in the space-charge-dominated regime.

This is a nice result because, comparing Eqs. (39) and (45), we see the correspondence of the kinematic and energy-conservation approaches in the space-charge-dominated regime. The kinematic approach includes information about the radial correlations; otherwise, they are equivalent.

C. Comparison of the emittance formulas with the numerical simulations, and discussion

Using Eq. (45), we predict that the maximum emittance growth is about 3.7×10^{-4} m, in reasonable agreement with Fig. 1(b). The error (about 40%) is probably due to the fact that there is both a quadratic and cubic component to the space-charge force. The maximum beam divergence after 2

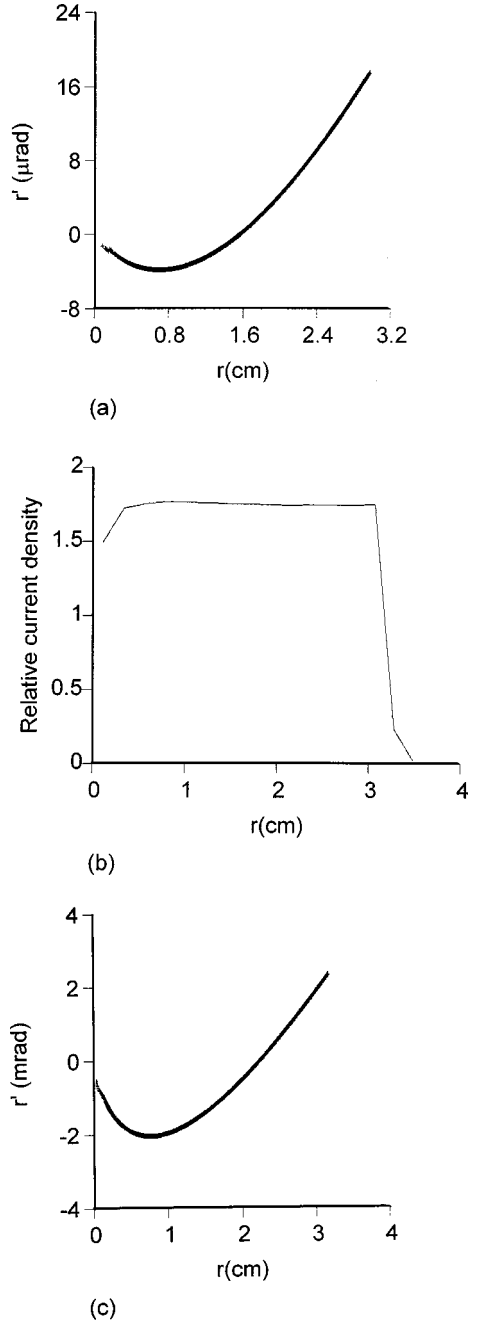

FIG. 4. (a) Phase space after 2 mm, (b) density profile at first emittance maximum, and (c) beam phase-space profile at first emittance maximum.

mm is shown in Fig. 4(a), and is 19 micro-radians, in good agreement with Eq. (21). In Fig. 4(b), we see the density profile at the first emittance maximum, and the profile is essentially uniform. Thus, all the excess potential energy has contributed to the emittance growth. In Fig. 4(c), we see the beam's radial phase space at the first emittance maximum. Its shape is similar to that in Fig. 4(a), as assumed in the kinematic model.

In Fig. 5 we show the emittance evolution for a 2-MeV, 4-kA beam. The maximum and equilibrium emittance are about 35% greater than for the 4-MeV, 4-kA beam (Fig. 1), demonstrating the energy scaling shown in Eqs. (39) and (45).

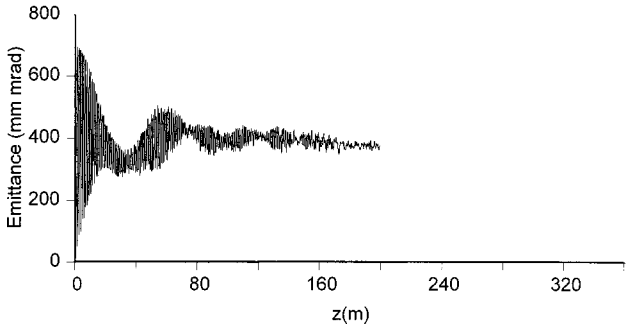

FIG. 5. 2-MeV, 4-kA case, emittance versus axial distance.

In Fig. 6 we show the emittance evolution for a 4-MeV, 2-kA beam. The maximum and equilibrium are about 40% lower than for the 4-MeV, 4-kA beam, also demonstrating the energy scaling shown in Eqs. (39) and (45). Note that the predicted increase in the plasma wavelength is seen.

Finally, in Fig. 7(a) we show the emittance evolution for a beam with a smaller effective initial density nonuniformity (about 30%), shown in Fig. 7(b). Equations (39) and (45) predict an emittance decrease of about 2.8 using these initial density nonuniformity magnitudes, in very good agreement with the decrease in the emittance in the simulation. Note that with the smaller effective current density nonuniformity, more plasma periods are required for the Landau damping.

Let us consider the form of Figs. 1(d) and 1(e). The emittance is still correlated in the equilibrium regime, but not correlated in the same way as initially, as shown in Figs. 4(a) and 4(c). However, we can reasonably assume that the correlations decrease the equilibrium emittance by a factor of $1/\sqrt{2}$, so the equilibrium emittance is about $\frac{1}{2}$ of the total allowable, uncorrelated emittance maximum, Eq. (39), as calculated using the excess potential energy. This leads to a prediction of 291 mm mrad for the equilibrium emittance, which is a good prediction of the result in Fig. 1(b).

Finally, note that the effect of having a significant uncorrelated emittance would be to prematurely mix up the correlations, leading to an earlier establishment of an equilibrium emittance. This effect does not occur in a strictly space-charge-dominated regime.

V. LONG-TERM EMITTANCE STABILITY

The final emittance thermalization feature we need to understand is the long-term stability of the equilibrium. From

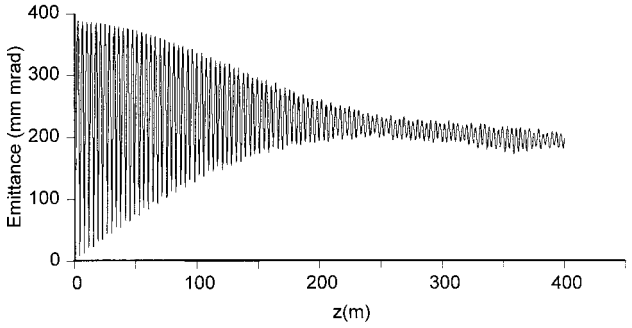

FIG. 6. 4-MeV, 2-kA case, emittance versus axial distance.

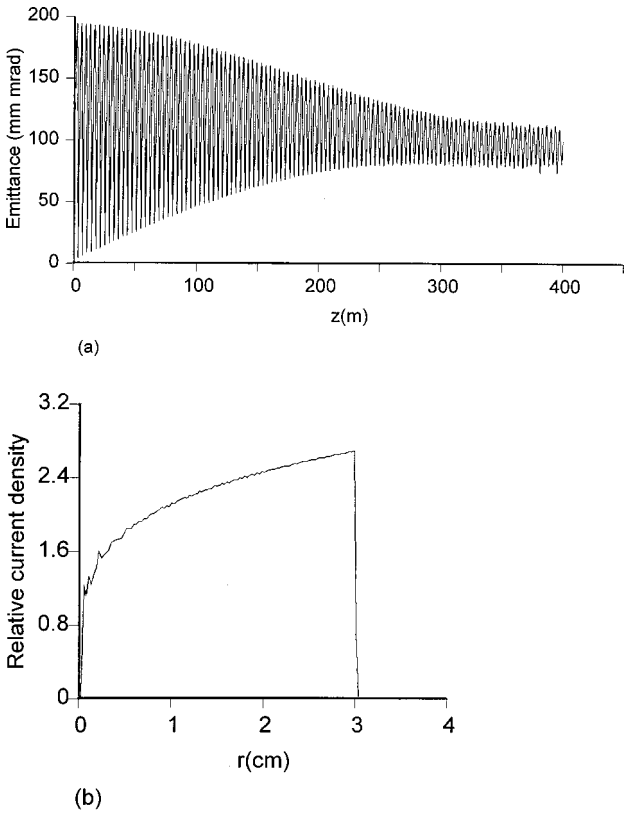

FIG. 7. (a) Emittance versus axial position for density nonuniformity of 30% and (b) initial density profile for density nonuniformity of 30%.

conservation of energy considerations, any change in the equilibrium emittance must occur from a transfer of energy between the radial and axial directions. In our problem, the external magnetic field is purely axial, and any transfer of energy must be due to the diamagnetic magnetic field.

The time integrated axial work on a given particle is

$$U_z = e \int B_r(r)\, \nu_\theta(r)\, dz, \tag{46}$$

where we use $r = r(z)$ over the particle's orbit. The azimuthal velocity is given by Busch's theorem,

$$\nu_\theta = -\frac{e}{\gamma m r} \int_0^r [B_{\mathrm{ext}}(r) + B_{z,\mathrm{dia}}(r)]\, r\, dr. \tag{47}$$

We write the diamagnetic axial field in terms of a Fourier decomposition

$$B_{z,\mathrm{dia}} = \sum_k \tilde{B}_{z,k} \cos(kz + \phi_k), \tag{48}$$

and the azimuthal velocity is

$$\nu_\theta = -\frac{e}{\gamma m r} \left\{ \frac{r^2}{2} B_{\mathrm{ext}} + \sum_k \cos(kz + \phi_z) \int_0^r \tilde{B}_{z,k}\, r\, dr \right\}. \tag{49}$$

Maxwell's equation for the divergence of the magnetic field gives us

$$B_{r,\mathrm{dia}} = \sum_k \frac{k}{r} \left(\int_0^r r \tilde{B}_{z,k}\, dr \right) \sin(kz + \phi_k). \tag{50}$$

Using $I_k = \int_0^r r \tilde{B}_{z,k}\, dr$, we rewrite the axial work as

$$U_z = -\frac{e}{\gamma m} \int \left\{ \frac{B_{\mathrm{ext}}}{2} \sum_k k I_k \sin(kz + \phi_k) + \frac{1}{r^2} \sum_k I_k \times \cos(kz + \phi_k) \sum_k k I_k \sin(kz + \phi_k) \right\} dz. \tag{51}$$

Note that each k term eventually averages to zero, including the constant $(k = 0)$ term. Thus, any long-term average exchange of energy between the axial to the transverse directions depends on correlations with the radial motion, which are small. This results in the long-term stability of the equilibrium emittance, as seen in Fig. 1(b).

ACKNOWLEDGMENTS

The author would like to acknowledge insightful discussions with Thomas Wangler and James Rosenzweig, who pointed out that wave breaking is an important limitation to coherent transverse plasma oscillations. This work was supported by funds from the Laboratory-Directed Research and Development program at Los Alamos National Laboratory, operated by the University of California for the U.S. Department of Energy.

APPENDIX: THERMALIZATION FROM WAVE BREAKING IN PHASE SPACE (EMITTANCE-DOMINATED REGIME)

The purpose of this appendix is not to provide a comprehensive analysis of the transition between the space-charge and emittance-dominated regimes. That is a complex issue and beyond the scope of this paper. Rather, it is to provide insight into understanding over what range of initial mismatches these emittance oscillations will occur for a beam with zero initial thermal emittance.

An important thermalization mechanism preventing emittance oscillations for many types of beams is wave breaking in phase space [16,17]. Wave breaking occurs when phase space becomes double valued, and the beam loses laminarity as kinetic energy is converted to potential energy. In that case, the radial correlations become mixed up and the emittance quits oscillating, leading to a thermalization effect. Because this wave breaking occurs during the first half of an emittance oscillation period, the characteristic time for thermalization is a quarter plasma period.

For the beams considered in this paper, this wave-breaking mechanism is negligible, but it does dominate for many cases, which have been studied in detail using the nonlinear free-energy approach [1,14,15]. In order to complete our understanding of the thermalization process for high-brightness induction linac electron beams, we need to understand the conditions where wave breaking leads to thermalization. First, we will consider the case where the initial emittance is zero, but the initial beam-current density is nonuniform. We will see that wave breaking only occurs at the radial edges of the distribution. Next, we will consider the

case where the initial density distribution is uniform, but there is some initial emittance leading to a curvature in phase space. From this approach, we will find the characteristic initial emittance that leads to wave breaking. For this case, wave breaking occurs when the initial phase-space curvature is large enough to overcome the space-charge repulsive force. In all cases, we will assume that the initial thermal emittance of the beam is zero.

Initial zero emittance case. For this case, we assume that the initial density distribution is nonuniform, but that the initial emittance is zero (the beam's distribution in phase space is a straight line). The approximate condition for wave breaking for a particle initially at a radius r is given by [17]

$$\int_0^r \nu\rho(\nu)d\nu > r^2\rho(r), \tag{A1}$$

where ν is a dummy variable of integration. Thus, wave breaking is present when the charge density drops to less than $\frac{1}{2}$ that of the average density out to that point. This condition is easy to derive, assuming that every particle has a radial equation of motion of the form

$$r'' = \alpha(\chi)\cos(k_p z), \tag{A2}$$

where χ is an index to keep track of each particle.

For a mostly matched, nearly uniform density beam, this condition does not occur, except in the radial tail of the distribution. Thus wave breaking will occur in the tail of a distribution heavily peaked on axis, but will not occur in the main body of a hollow distribution, as we have seen in the previous numerical simulations.

Uniform initial density case. For the second case, we assume that the density is uniform, but that there is an initial beam emittance. There are an infinite number of possible initial configurations in radial phase space with a given emittance; for simplicity, we will assume the beam is an ellipse in phase space, where the beam divergence obeys

$$r'^2 = (r_e^2 - r^2)\frac{\varepsilon^2(2\beta\gamma)^2}{r_e^4}. \tag{A3}$$

Using the assumed form for the radial equation of motion, Eq. (A2), we find that wave breaking for this case occurs if $dr/d\chi = 0$, or

$$\chi = \frac{r_e}{\left[1 + \left(\frac{\varepsilon}{2\beta\gamma r_e^2 k_p}\sin(k_p z)\right)^2\right]^{1/2}}. \tag{A4}$$

Note that wave breaking will always occur for any nonzero emittance, but only right at the edge of the beam for small emittances. For thermalization of the bulk of the beam, the wave breaking needs to occur in the middle of the beam, or the emittance must exceed the characteristic value of

$$\varepsilon_{w-b} = 4r_e\sqrt{(I/I_A)/\gamma\beta}. \tag{A5}$$

For the case studied in this paper, this characteristic emittance is about 0.02 m, which is nearly two orders of magnitude larger than the actual emittances induced by the density nonuniformity. Thus, thermalization due to wave breaking is negligible in the case considered. Note that the parameters scale the same as in Eqs. (39) and (45), and that the emittance from a density nonuniformity of the type studied in this paper will never exceed the wave-breaking characteristic value.

For comparison, we calculate the wave-breaking characteristic emittance for a hydrogen-ion beam, with $\gamma \sim 2$. For a beam current of 100 mA and a beam radius of 1 mm, the characteristic wave breaking emittance is less than 0.2 mm mrad. Thus, thermalization due to wave breaking is a much more common phenomena for beams in that regime.

[1] M. Reiser, *Theory and Design of Charged Particle Beams* (Wiley, New York, 1994).

[2] B. E. Carlsten, Phys. Rev. E **58**, 2489 (1998).

[3] B. E. Carlsten, Nucl. Instrum. Methods Phys. Res. A **285**, 313 (1989).

[4] X. Qiu, K. Batchelor, I. Ben-Zvi, and X-J. Wang, Phys. Rev. Lett. **76**, 3723 (1996).

[5] L. Serafini and J. B. Rosenzweig, Phys. Rev. E **55**, 7565 (1997).

[6] B. E. Carlsten and D. T. Palmer, Nucl. Instrum. Methods Phys. Res. A **425**, 37 (1999).

[7] P. Allison, Los Alamos National Laboratory, DARHT Report Note 42, 1993 (unpublished).

[8] P. Allison, D. Moir, and G. Sullivan, Los Alamos National Laboratory Report DARHT Technical Note No. 58, 1996 (unpublished).

[9] B. E. Carlsten, Phys. Plasmas **5**, 1148 (1998).

[10] J. F. Gittens, *Power Traveling-Wave Tubes* (Elsevier, New York, 1965).

[11] H. Boersch, Z. Phys. **139**, 115 (1954).

[12] W. Knauer, Optik **54**, 211 (1979).

[13] H. Rose and R. Spehr, Optik **57**, 339 (1980).

[14] D. Kehne, M. Reiser, and H. Rudd, in *Proceedings of the 1991 Particle Accelerator Conference*, edited by Loretta Lizama and Joe Chew (IEEE, New York, 1991), p. 248.

[15] A. Cucchetti, M. Reiser, and T. Wangler, in *Proceedings of the 1991 Particle Accelerator Conference* (Ref. [14]), p. 251.

[16] J. Rosenzweig (private communication).

[17] O. A. Anderson, Part. Accel. **21**, 197 (1987).